8-22-2018

Open-source Tools for Dense Facial Tissue Depth Mapping (FTDM) of Computed Tomography Models

Terrie Simmons-Ehrhardt
School of World Studies, Virginia Commonwealth University, terrielsimmons@gmail.com

Catyana Falsetti
School of Geological Sciences & Urban Planning, Arizona State University

Anthony B. Falsetti
School of Mathematics and Natural Sciences, Arizona State University

Christopher J. Ehrhardt
Department of Forensic Science, Virginia Commonwealth University

Open-source Tools for Dense Facial Tissue Depth Mapping (FTDM) of Computed Tomography Models

Terrie Simmons-Ehrhardt,[1]* Catyana Falsetti,[2] Anthony B. Falsetti,[3] and Christopher J. Ehrhardt[4]

[1]School of World Studies, Virginia Commonwealth University, Richmond, Virginia, USA.

[2]School of Geological Sciences & Urban Planning, Arizona State University, Tempe, Arizona, USA.

[3]School of Mathematics and Natural Sciences, Arizona State University, Glendale, Arizona, USA.

[4]Department of Forensic Science, Virginia Commonwealth University, Richmond, Virginia, USA.

*Correspondence to: Terrie Simmons-Ehrhardt, School of World Studies, Virginia Commonwealth University, 312 N. Shafer St., Richmond, VA 23284 USA. E-mail: terrielsimmons@gmail.com.

Short Title: Dense Facial Tissue Depth Mapping of CT Models

KEY WORDS: FORENSIC SCIENCE, FORENSIC ANTHROPOLOGY, FACIAL APPROXIMATION, FACIAL TISSUE DEPTH MAPPING (FTDM), COMPUTED TOMOGRAPHY (CT), FORENSIC ART, CRANIOFACIAL IDENTIFICATION, MESHLAB

Abstract

Computed tomography (CT) scans provide anthropologists with a resource to generate three-dimensional (3D) digital skeletal material to expand quantification methods and build more standardized reference collections. The ability to visualize and manipulate the bone and skin of the face simultaneously in a 3D digital environment introduces a new way for forensic facial approximation practitioners to access and study the face. Craniofacial relationships can be quantified with landmarks or with surface processing software that can quantify the geometric properties of the entire 3D facial surface. This paper describes tools for the generation of dense facial tissue depth maps (FTDMs) using de-identified head CT scans of modern Americans from the public repository, The Cancer Imaging Archives (TCIA), and the open-source program Meshlab. CT scans of 43 females and 63 males from TCIA were segmented and converted to 3D skull and face models using Mimics and exported as stereolithography (STL) files. All subsequent processing steps were performed in Meshlab. Heads were transformed to a common orientation and coordinate system using the coordinates of nasion, left orbitale, and left and right porion. Dense FTDMs were generated on hollowed, cropped face shells using the Hausdorff sampling filter. Two new point clouds consisting of the 3D coordinates for both skull and face were colorized on an RGB scale from 0.0 (red) to 40.0 mm (blue) depth values and exported as polygon file format (PLY) models with tissue depth values saved in the "vertex quality" field. FTDMs were also split into 1.0 mm increments to facilitate viewing of common depths across all faces. In total, 112 FTDMs were generated for 106 individuals. Minimum depth values ranged from 1.2 mm to 3.4 mm, indicating a common range of starting depths for most faces regardless of weight, as well as common locations for these values over the nasal bones, lateral orbital margins, and forehead superior to the supraorbital border. Maximum depths were found in the

buccal region and neck, excluding the nose. Individuals with multiple scans at visibly different weights presented the greatest differences within larger depth areas such as the cheeks and neck, with little to no difference in the thinnest areas. A few individuals with minimum tissue depths at the lateral orbital margins and thicker tissues over the nasal bones (> 3.0 mm) suggested the potential influence of nasal bone morphology on tissue depths. This study produced visual quantitative representations of the face and skull for forensic facial approximation research and practice that can be further analyzed or interacted with using free software. The presented tools can be applied to pre-existing CT scans, traditional or cone-beam, adult or subadult individuals, with or without landmarks, and regardless of head orientation, for forensic applications as well as for studies of facial variation and facial growth. In contrast with other facial mapping studies, this method produced both skull and face points based on replicable geometric relationships producing multiple data outputs that are easily readable and software that is openly accessible.

The analysis of facial tissue thickness has important implications for forensic anthropology and, specifically, the procedures used to create facial approximations of unidentified human remains. Traditional tissue depth studies have collected data from a limited number of points on the face using various manual sampling methods and a variety of world populations, beginning with needle puncture of cadavers by His (1895, cited in (Stewart 1954)) and Kollmann and Buchly (1898, cited in (Krogman and Iscan 1986), and continuing even until very recently (Suzuki 1948; Rhine and Campbell 1980; Rhine and Moore 1984; Simpson and Henneberg 2002; Domaracki and Stephan 2006; Codinha 2009; deAlmeida et al. 2013). Ultrasound methods eventually gained favor given the ability to capture *in vivo* data in an upright position: (Hodson et al. 1985; El-Mehallaway and Soliman 2001; Wilkinson 2002; De Greef et al. 2006; Stephan and Simpson 2008; Manhein et al. 2000; Huculak and Peckmann 2012; Baillie et al. 2015; Jia et al. 2016; Stephan and Preisler 2018). Cephalograms and radiographs have been used primarily to collect midsagittal profile depths: (Dumont 1986; Smith and Buschang 2001; Williamson et al. 2002; Utsuno et al. 2014; Brierset al. 2015; Jeelani et al. 2015; Kotrashetti and Mallapur 2016). Three-dimensional data from computed tomography (CT), cone-beam CT, and MRI have become more prevalent, given the increasing access to pre-existing data and availability of computing resources: (Phillips and Smuts 1996; Hwang et al. 2012; Dong et al. 2012; Panenkova et al. 2012; Guyomarc'h et al. 2013; Ruiz 2013; Parks et al. 2014; Bulut et al. 2014; Sipahioglu et al. 2012; Starbuck et al. 2015). Studies have also applied a combination of methods (Aulsebrook et al. 1996). Regardless of the imaging modality, the morphological and quantitative association between the bone and skin landmarks in these point-centric data collection methods is often unclear, affecting not only the accuracy of the data, but also preventing inter-study comparisons and replication. A recent paper has proposed recommendations for bone and skin landmark pairs

for application in craniofacial identification methods, but even this list contains pairs that do not necessarily exist at 90^0 to each other or have not had consistent positional relationships established to each other (Caple and Stephan 2016). Even with modern medical imaging and the ability to simultaneously visualize bone and skin in correct anatomical orientation to each other in CT scans, the collection of skin points at a 90^0 angle from corresponding bone points, as recommended by His (Stewart 1954) (Krogman and Iscan 1986) is still difficult to achieve by manual point placement (Hwang et al. 2015) and will continue to be difficult until consistent positional relationships between bone and skin landmarks have been quantified and established regardless of the direction of measurement (bone landmarks to skin or skin landmarks to bone).

The development and availability of 3D processing software has expanded the number of analytical methods that can be applied to the 3D skull and face surface models that can be reconstructed from CT scans. The 3D meshes contain geometric properties that can be quickly quantified by accessible software. These programs can also facilitate unique training and educational opportunities by allowing the development of interactive 3D resources to provide practitioners access to immersive craniofacial data. Utilizing algorithms and processing tools that are commonly applied for 3D model comparisons, it is now possible to build a high quality, interactive reference database for craniofacial identification research and applications. While the application of mesh processing algorithms to facial CT scans is not new, the application/extraction of dense facial tissue depths has primarily been part of the development of automated and/or statistical facial approximation computer programs (Tu et al. 2005; Turner et al. 2005; Vandermeulen et al. 2006). As such, the tools themselves have existed as part of the developed software rather than as external tools available to other researchers or practitioners. More recent studies have applied dense facial tissue depth mapping to CT scans, but have not

produced the corresponding skull points (Shrimpton et al. 2014) or designated a collection between face and skull points at the same z-coordinate after orientation to the Frankfurt Horizontal plane (Shui et al. 2016). Shrimpton et al. (2014) specifically state that although a user could pick a point on the face to view a specific tissue depth on their regressed face maps (TDMorpheus©), the corresponding bone point would be unknown to the user. Shui et al. (2016) generated both skull and face points, but the collection of skull and face points at the same z-coordinate ignores the curvature of both surfaces and is orientation-dependent. From these studies, it should be possible to extract facial tissue depth data in a dense, more objective/automated manner utilizing CT scans, but there is still a need for a method to provide both bone and skin points that can be identified as corresponding, to be orientation-independent, and to be widely accessible.

An added problem is that facial approximation practitioners are traditionally presented with these tables of sparse-point tissue depth data consisting primarily of averages to create facial approximations with little to no information regarding the contours of tissue depths within a face or how to adjust faces for weight, other than to apply global increases by adding one or two standard deviations to each landmark, which may not be a biologically accurate representation of weight changes. Practitioners could benefit from having access to data that is more intuitive, easily interpretable, and interactive, rather than relying on traditional data such as pooled tissue depth tables, (Stephan and Simpson 2008; Stephan 2017; Stephan 2017), or raw tissue depth point data that have been made freely available (e.g., www.craniofacialidentification.com).

To expand on previously published studies and further utilize the geometric properties of 3D surfaces and the availability of open-source surface processing technologies, this paper

presents a method for dense facial tissue depth mapping (FTDM) that 1) eliminates several sources of error known to manual point collection methods and 2) produces quantitative data for both bone and skin in an accessible, interactive, and intuitive visual format. We describe a method for objective calculation of dense FTDMs using the Hausdorff sampling filter in Meshlab (Cignoni et al. 1998; Aspert et al. 2002; Cignoni et al. 2008). This distance is commonly used as a method for comparing two meshes in 3D modeling applications including the stand-alone 3DMeshMetric (http://www.nitrc.org/projects/meshmetric3d/) and the "ModelToModel Distance" plug-in option in 3D Slicer (https://www.slicer.org/; Fedorov et al. 2012). We have utilized this filter to find the closest point on the bone for every point on the face. Our step-by-step procedure, with accompanying Meshlab scripts, is downloadable as a user guide (Simmons-Ehrhardt et al. 2017). This method produces 3D coordinates for bone and skin points, regardless of orientation of the CT scan, utilizing freely available software and can be applied to any 3D head models (as long as the skull and face models are in correct anatomical orientation to each other; models generated from the same CT scan will be). The publication of this method and toolset can facilitate collaborations between forensic researchers and practitioners towards the development of a standardized, accessible reference database for craniofacial identification.

Materials and Methods

CT Preparation. This study is part of a larger effort utilizing de-identified, publicly available head CT scans from a web-based repository, The Cancer Imaging Archives (TCIA) (http://www.cancerimagingarchive.net/; Clark et al. 2013), to investigate bone to skin relationships for craniofacial identification applications. Collections included in this study

include the Head-Neck Cetuximab collection (Bosch et al. 2015), QIN-HEADNECK collection (Beichel et al. 2015; Fedorov et al. 2016), The Cancer Genome Atlas Head-Neck Squamous Cell Carcinoma (TCGA-HNSC) collection (Zuley et al. 2016), and The Cancer Genome Atlas Thyroid Cancer (TCGA-THCA) collection (Kirk et al. 2016). The research protocol was submitted to Virginia Commonwealth University's Institutional Review Board and found to be exempt from human subjects review. Table 1 lists the sex distributions of the sample and Figure 1 shows the age distribution.

CT scans containing head data were downloaded and segmented into separate soft tissue and bone masks using Mimics© v. 17.0 (Materialise, Leuven, Belgium). Although Mimics was used to generate 3D models for further study with other measurement modules within Mimics, the models required for tissue depth mapping could be generated with free CT processing software, such as 3DSlicer (https://www.slicer.org/; Fedorov et al. 2012), for which many online user resources exist. CT scan resolutions varied from 1.0 mm slice thickness (0.5 mm slice increment) up to 5.0 mm slice thickness (2.4 mm slice increment), but the majority of scans were at 3.0 mm slice thickness (2.0 mm slice increment) and 3.75 mm slice thickness (3.27 mm slice increment). The default threshold of 226 Hounsfield units was applied to separate bone from soft tissue, but adjusted per individual for lower bone density as needed (i.e., lowered for scans showing lower bone density), and local thresholding was applied to improve rendering of areas of thin/less dense bone such as the maxillae. A built-in imaging filter was applied to scans with grainy images to produce cleaner segmentation masks. Vertebrae and artifacts such as dental streaks were removed using the multi-slice edit tool to select and erase unwanted pixels. The soft tissue mask was segmented using the default soft tissue value (< 226) and cropped below the chin. The soft tissue mask was also edited to attempt to fill holes and remove artifacts as needed.

The final edited bone mask was subtracted from the edited soft tissue mask using the Boolean tool to produce a new soft tissue mask that did not have overlapping pixels with the bone mask (local editing of the bone mask may have resulted in the segmentation of pixels that would have been thresholded under the soft tissue value of < 226). 3D face and skull models were reconstructed from the 2D segmentation masks using a custom setting (not the "Optimal" setting) with the following parameters: Gray Value Interpolation, 10 smoothing iterations with a smooth factor of 0.300, shell reduction of 1 (to eliminate disconnected pieces). No matrix reduction or triangle reduction was applied, so models contained the largest possible number of vertices/triangles based on CT scan resolution.

As part of the larger study, landmarks were placed on the 3D skull and face models using the simulation module in Mimics and x-, y-, z-coordinates for the landmarks were exported. 3D stereolithography (STL) models of the skull and face were exported for further processing in Meshlab. The coordinates for nasion (N), left orbitale (OrL), and left and right porion (PoL and PoR) were used to calculate rotations and a translation to position each head into a standardized orientation and coordinate system. Three reference planes were selected for alignment, the Frankfurt Horizontal (FH) plane through OrL, PoL, and PoR, a coronal plane passing through PoL and PoR, and a mid-sagittal plane through N (Figure 2). The coordinate system consists of the x-axis representing the medial-lateral direction (anatomical left of N = positive), y-axis representing the anterior-posterior direction (anterior to PoL/PoR = negative), and z-axis representing the superior-inferior direction (superior to FH = positive). The formulae involved calculating a rotation to align PoL and PoR to the same z-coordinate, then PoL and PoR to the same y-coordinate, then OrL to the z-coordinate of PoL and PoR, and finally a translation from the x-coordinate of N, y-coordinate of PoL/PoR, and z-coordinate of OrL/PoL/PoR. This resulted

in a coordinate system of N at x = 0, PoL and PoR at y = 0, and OrL, PoL, and PoR at z = 0. One transformation per head was calculated and applied to the bone and skin models for an individual. The set of rotations and final translation were applied in Meshlab to the 3D bone and skin STL models. This system was chosen to allow heads to be viewed in the same 3D space in any viewer such as Meshlab or 3DSlicer, in the same orientation consistent with those utilized in craniofacial identification methods. The spreadsheet and Meshlab scripts for performing this transformation have been made available for download (Simmons-Ehrhardt et al. 2017). Transformed skull and face models were saved and re-imported into Meshlab v.1.3.3 for tissue depth mapping. Although we chose to orient the head models to a common orientation and coordinate system, this step is not required in order to generate dense FTDMs. The heads we utilized had widely ranging coordinate systems due to some of the scans extending beyond the head which made viewing of more than one head at a time within one software window difficult.

We have made available a user guide detailing the steps within Meshlab to prepare a face model and the method for facial tissue depth mapping (Simmons-Ehrhardt et al. 2017). Figure 3 summarizes the steps outlined in the user guide and described briefly below.

Model Editing. Because the soft tissue segmentation of the CT data includes all of the soft tissue voxels, the face model contains internal surfaces connected to the external surface that need to be removed before mapping in order to create a "face shell". A sequence of filters in Meshlab was implemented to apply shading to the model, select and delete internal surfaces based on the shading values, and remove remaining disconnected pieces. The hollowing of the face model may be performed in other software as long as a "face shell" consisting of only an outer surface is obtained. In order to reduce the model even further to isolate only the face, we

defined an area based on a user-selected distance from pronasale, as identified in the simulation module of Mimics, that extended just posterior to the gonial angle but anterior to the external auditory meatus. Although the entire hollowed face shell may be used for tissue depth mapping, we chose to map an area consisting primarily of the face, while excluding the ears, much of the neck, and attempting to minimize distorted tissues just anterior to the ears. Cropping the face anterior to the ears is not necessary to generate dense FTDMs: the entire head can be mapped as long as there are no disconnected pieces and the face is only an external shell.

Tissue Depth Mapping. The transformed skull STL and the hollowed, cropped face STL were imported into a new Meshlab v.1.3.3 project for facial tissue depth mapping. The "Hausdorff Distance" Sampling method was selected from the Filter menu. The face model was selected as the Sampled Mesh, and only vertices were selected for sampling, so that the number of points measured was equal to the number of vertices in the face model. For very high resolution CT scans, this value was excessively high and required prolonged computation time (minutes vs. seconds). In these cases, we decimated the skull and face meshes with the Quadratic Edge Collapse filter before tissue depth mapping. The "Max Distance" in the sampling window was set at 40 mm to adequately cover all facial thicknesses.

After sampling was completed, the original face mesh as well as two Hausdorff point clouds consisting of the actual measured skull points (Hausdorff Closest Points) and face points (Hausdorff Sample Points) were colorized and exported as PLY files. Because the depth value was stored in the vertex quality field of the PLY model, this value was used to standardize the color maps from 0 mm (red) to 40 mm (blue), before export (the default colorization is from minimum to maximum vertex quality values). PLY models were also saved in ASCII format so

that they could be opened in a text editor to read x-, y-, z- coordinates, vertex normals, RGB color values, and tissue depth values saved in the vertex quality field (last column). In the Hausdorff point clouds, the corresponding points are listed in the same order between the skull and face models.

Viewing Data. In order to subdivide the tissue depth data into smaller areas, we segmented the skull and face Hausdorff point clouds into 1.0 mm increments (0-0.5 mm, 0.5-1.5 mm, 1.5-2.5 mm, etc.). To quickly generate these incremental maps, we saved the sequence of Meshlab filter scripts needed to split a face/skull model and created a batch script to call up Meshlabserver.exe to save the depth increments as separate PLY files (Hazelden 2014). We have provided a zip file containing scripts needed to split the mapped face and skull points into all 1.0 mm increments (from 0 mm to 40 mm), as well as merge the corresponding face and skull points at each depth increment so that corresponding face and skull points for one increment can be viewed simultaneously as one PLY model (see Figure 3). Details for installing and running the scripts can be found in Appendix II of the user guide (Simmons-Ehrhardt et al. 2017). Depth values for specific points can also be viewed by using the "Get Info" button in Meshlab 2016 and clicking on the mapped and colorized PLY face mesh to produce an on-screen label of x-, y-, z-coordinates and depth (labelled Q). Additional viewing options in Meshlab include rendering the "Quality Contour" to generate contour lines on the face where the depth values change, essentially a topographic map of the face.

Results

We generated 112 sets of FTDMs for 106 individuals. Sampled face meshes ranged in resolution from 19,377 vertices to 202,659 vertices and took from 0.81 sec to 87 sec to map, with an average of 8.3 sec. Faces with fewer than 100,000 vertices (n = 102) took from 0.81 to 12.9 sec to map and averaged 4.6 sec. Two individuals with a CT slice thickness of 1.0 mm and slice increment of 0.50 mm had to be decimated using the Quadratic Edge Collapse filter in Meshlab in order to perform mapping in a reasonable amount of time. A few models were tested through 3DMeshMetric's sampling method as well as the Model to Model Distance tool in 3DSlicer and the same distances were obtained. However, both programs export the distance data in the VTK file format and do not give as many customization options for colorization or point cloud exports. 3DMeshMetric also could not sample high resolution models.

The minimum tissue depth values for all maps combined ranged from 1.2 mm to 3.4 mm. Observations of the incremental maps indicated that the thinnest tissues occurred most frequently on the lateral surfaces of the nasal bones with slightly thicker tissues over the top of the nasal bones, including rhinion. Depths of < 5.0 mm most commonly occurred over the nasal bones, forehead (superior to the supraorbital border), lateral orbital margins and sometimes along the mandibular border and inferior orbital margin. A few individuals for whom the thinnest tissues occurred at the lateral orbital margins rather than over the nasal bones (nasal bone depths were > 3.0 mm) were not the heaviest individuals but rather seemed distinguished by the morphology of their nasal bones, which indicated possible African ancestry. Although the age range of our sample was not well distributed and the scans varied in completeness of facial surface area, our preliminary data suggest that a higher proportion of thinner tissues may be present in older individuals, especially over the forehead. Maximum values occurred at pronasale or at the cheeks and in the neck for the heaviest individuals.

Five individuals in our dataset had more than one CT scan showing visibly different weights (Figures 4 and 5). In intra-subject comparisons, differences were observed most notably in the cheeks, along the mandibular border and zygomatic arches. Weight loss was indicated by a higher proportion of red (< 5.0 mm), occurring along the mandible, zygomatic arches, and sometimes over the forehead. In the heavier scans, the tissues over the nasal bones, lateral orbital margins, and forehead were not necessarily thicker than in the scans from a lower body weight, especially over the nasal bones. The heavier scans did not always have larger minimum tissue depths, with differences ranging from -0.24 mm (negative indicates smaller value for heavier face) to 0.37 mm (positive indicates larger value for heavier face). Figure 5 shows one individual for whom we processed 3 scans with visibly different weights, especially evident in the overall roundness of the face and neck folds (5a is the thinnest, 5b is the next heaviest, and 5c is the heaviest). Quality contour lines were also added to highlight depth transition lines. With increased weight, there was an increase in the neck folds and a decrease of thinner tissues along the mandibular border, especially noticeable in the chin area. Interestingly for this individual, the nose appeared slightly wider as well in the heavier face, indicating that weight may affect facial feature dimensions, most likely due to the supine position.

Discussion

Regardless of the methods applied to collect facial tissue depths, there have always been intrinsic limitations to both the accuracy and reproducibility of the data, mostly because of the multiple opportunities for observer error. For manual methods, depth measurements can be hampered by the inability to see bone under the skin, and for CT-based methods where the bone can be visualized under the skin, there is disagreement as to whether the measured bone and skin

landmarks should be perpendicular to each other or measured between specific anatomical landmarks or even whether bone or skin landmarks should be used as the reference. There are also issues with reproducibility, depending on which landmark definitions are used (Hwang et al. 2015). Other groups have cautioned that CT collection of FSTD data has a number of potential sources of error and that as many of those as possible should be minimized (Caple et al. 2016). The method presented here eliminates several sources of error including the effect of head position and the manual identification of landmarks. Although we chose to transform the head models to a common orientation by aligning N, PoL, PoR, and OrL, this transformation is not necessary in order to follow the workflow outlined here to generate dense FTDMs. The consistent anatomical orientation of face to skull would result in the same tissue depth maps regardless of the orientation of the head itself; head orientation does not matter as the mapping only considers the two surfaces relative to each other. In addition, the cropping of the face to a distance from Prn is also not a necessary step, as the soft tissue of the entire head could be sampled to the skull. Figure 6 depicts a wireframe mesh of a mapped full head (hollowed face shell) with skull points visible through the mesh. The only necessary steps are generating corresponding face and skull 3D models from the same CT scan and hollowing and cleaning the face model to produce a single external facial shell.

Although the dense FTDMs would be a more advantageous output over conventional sparse-point methods, the tools presented here could also be applied to either generate landmark-based depths in a more standardized and repeatable manner or to collect point-based tissue depths from the FTDMs themselves. The distance filter itself can be applied to two surfaces or to a landmark set and a surface (skin landmarks to a skull surface or vice versa). Given the quantitative nature of the 3D surfaces, any observer with the same landmark coordinates and

surfaces would produce the same values. Landmark-based data could also be collected from the dense FTDMs by utilizing the "Get Info" button in Meshlab 2016 to read the vertex index, coordinates, depth, and color, and then utilizing the conditional vertex selection filter to locate the corresponding bone point with the same vertex index. The distances can also be performed in either direction, from face to skull or from skull to face. However, in our preliminary evaluations of directionality, measuring from the skull surface to the face results in large unsampled portions of the face (Figure 7). In addition, sampling from the skull produces points on the face that were measured from impractical surfaces on the skull. By sampling from the face to the bone, we are ensuring that 1) all of the face is measured and 2) that each measured point on the face has a usable and retrievable point on the bone. Because the Hausdorff distance filter utilizes each point on the sample model (face) and finds the closest points on the target model (skull), certain parts of the skull are not referenced at all, and others may have duplicate skull points that were measured from different skin points. The skull areas that are not measured are deep or recessed areas from which measurements would not be logical to collect or on which tissue depth markers could not physically (or digitally) be placed (Figure 8). In addition, generating a "skull shell" to exclude internal surfaces would be much more difficult than generating a face shell. We are currently evaluating distances generated from traditional tissue depth markers in both skull-to-face and face-to-skull directions to determine for which landmarks the direction of measurement would not significantly affect the depth value, although arguably, nearly all tissue depth collection methods have measured from the face to the skull. As part of our larger study, we are also generating data regarding facial feature dimensions and positions which will provide more information about the strength/consistency of associations between bone and skin landmarks that are utilized in tissue depth studies. It seems likely that

some bone and skin landmarks will have a closer association to each other so that the direction of measurement does not significantly affect the depth value, such as zygion, glabella, nasion, gonion, since the soft tissue points are defined as directly overlying these bone points. In comparing multiple tissue depth studies, it becomes apparent that some bone and skin landmarks that are presented for application in traditional tissue depth tables do not always occur perpendicular to each other and that local curvatures of the craniofacial skeleton can vary greatly among individuals, affecting the ability to collect specific landmarks at consistent locations to each other via manual methods or even to place tissue depth markers. For example, the more developed supraorbital ridge in males results in an inferiorly directed surface, or overhang, just superior to nasion, whereas this area tends to be less developed and flat in the female skull. This difference is highlighted in Figure 8 where the male skull has no sampled points around nasion because of the development of the supraorbital ridge; the closest bone points to the skin in this area occur on the supraorbital ridge and more anteriorly along the nasal bones. Other inter-individual curvature differences would be most likely to occur along the midsagittal landmarks, making it nearly impossible to either collect landmark-based measurements consistently among individuals or place tissue depth markers consistently in practice. Another concern is the potential for duplicate bone points per multiple skin points, especially in cases where bone may be missing due to pathology or alveolar resorption, but the ability to retrieve and visualize the corresponding bone point would provide a reference even in such cases. However, these individualizing differences can be accounted for by utilizing a repeatable geometric measurement of the bone and skin surfaces, such as through the FTDM method outlined here. The measurements in either direction, skull to face or face to skull, can be collected objectively

in order to search for consistent positional relationships. The visualization of contour maps (Figure 3d) may also assist with identifying informative points.

The primary limitation of this study is the use of supine CT scans that have varying degrees of tissue distortion in the cheeks (Baillie et al. 2015; See et al. 2008). A recent study found that for individuals of average body mass index, distortion in the buccal, masseteric, and nasiolabial regions exceeded 2 mm difference in tissue thicknesses between laser scans of supine and upright faces, with buccal and masseteric regions being thicker and the nasiolabial regions being thinner in the supine faces (Bulut et al. 2017). Given the variability among faces for individuals with more than one scan in our sample (Figures 4 and 5), it may be that a certain amount of intra-subject error is to be expected, even when the compared scans are both supine. Notably, the tissue depths from this study did not show a uniform increase over the entire face in the heavier scan of an individual. Heavier faces still had similarly thin tissues over the nasal bones, lateral orbital margins, and forehead, although for one individual (Figure 5), increased weight also seemed to expand the width of the nose slightly. This suggests that the supine position may not only affect tissue depths but facial feature dimensions as well, though whether to a degree that would affect biometric facial recognition has yet to be demonstrated. The methods presented here greatly facilitate the comparison of scans for one individual to assess the degree of intra-subject variation expected in FTDMs.

The quality of 3D models will likely have an effect on the FTDM as low resolution CT scans will result in 3D meshes with fewer vertices. However, the ability to map every vertex of the face model, on the order of tens of thousands of points, may minimize the effects of low CT resolution. The greatest effect of low resolution CT scans would be on the representation of detailed facial features and on the quality of the bone data, as many structures will not properly

segment and render, especially areas of thin bone such as the maxillae. The skin of lower resolution CT scans will render but may suffer from stepping artifacts and/or less defined features. On the other hand, CT scans with high resolution will result in models with hundreds of thousands or millions of points, resulting in increased and potentially prohibitive computation times requiring decimation to fewer points prior to mapping. As mentioned above, the outlining of our methods and the tools available would allow for further studies into how many points would be needed to accurately represent a face. Because our collection came from pre-existing CT scans of varying resolutions, we are evaluating the standardization of the resultant maps for further statistical analyses. Standardizing the number of points per head would allow the development of more surface statistics and the generation of deformable models. However, it might be most prudent to collect dense FTDMs from the highest resolution models attainable from a particular CT scan protocol and then sub-sampling a regular interval or point cloud number to standardize a collection so as not to inadvertently impose any geometric inaccuracies (large mesh triangles) on the mapping procedure. As the segmentation of the CT scans into bone and skin models requires the most user input and therefore the most opportunity for error, the goal would be to generate the most anatomically accurate representations of the original CT data.

This method for generating dense FTDMs will allow researchers working with head CT scans to easily and quickly generate foundational data to supplement facial approximation methods. Dense FTDMs from existing CT scans will provide facial approximation practitioners and researchers a valuable resource to study tissue depth variation on actual interactive 3D faces rather than solely as data tables. Future work based on the data in this study will include the production of interactive tools for practitioners and possibly a plug-in for Meshlab to consolidate the relevant tools. Until then, all tissue depth data and even landmark locations can be generated

with and visualized in Meshlab. Visual and quantitative datasets can be produced for adults and subadults, yielding resources not only for forensic applications, but also for studying facial variation and facial growth. The advantage of producing both bone and skin points is the eventual possibility of statistically estimating FTDMs for unidentified skulls based on individual craniofacial morphology. For facial approximation practitioners, the smaller incremental maps provide a more accessible way to visualize the contours of an individual face, from thinnest to thickest tissues, and will potentially improve the methods for generating facial approximations. All data for one head can be viewed simultaneously as layers in Meshlab: this includes the original skull and face models (STL), the mapped and colorized facial surface (PLY), the mapped and colorized bone and skin Hausdorff point clouds (PLY), the incremental (1.0 mm) face and skull point clouds (PLY), and even 3D landmark coordinates (XYZ). Through workshops and the development of online interactive resources, the application of these maps for training of facial approximation practitioners will greatly enhance their ability to visualize facial contours and provide a more intuitive and immersive way of studying the face.

Perspectives

In comparison to other efforts to produce dense FTDMs, the workflow outlined here utilizes accessible, open-source tools to generate and interact with FTDMs, and produces coordinates of the bone points that are closest to the sampled skin points. Such mapping allows for a more comprehensive approach to viewing tissue depth contours within one individual and between individuals and will potentially reveal more informative tissue depth regions for facial approximation methods. With the increased accessibility of CT data, the ability to take advantage of 3D surface processing methods, especially with free software, eliminates the need for facial

approximation studies to rely on potentially inaccurate, manually-landmarked FSTD data. We present this method to facilitate the standardized generation of dense FTDMs from pre-existing 3D head models or CT scans and to promote a uniform method of data collection in an effort to improve the quality of reference data available to facial approximation researchers and practitioners. By providing our step-by-step workflow, we invite other researchers to apply the methods and promote discussions of how best to standardize reference data for craniofacial identification methods and improve access of these data to researchers and practitioners.

Acknowledgements

This project was supported by Award No. 2014-DN-BX-K005, awarded by the National Institute of Justice, Office of Justice Programs, U.S. Department of Justice. The opinions, findings, and conclusions or recommendations expressed in this publication/program/exhibition are those of the author(s) and do not necessarily reflect those of the Department of Justice.

Received 8 January 2018; revision accepted for publication 22 May 2018.

Literature Cited

Aspert, N., D. Santa-Cruz, and T. Ebrahimi. 2002. MESH: Measuring errors between surfaces using the Hausdorff distance. *Proc. (IEEE Int. Conf. Multimed. Expo)* 1:705–708.

Aulsebrook, W. A., P. J. Becker, and M. Y. Iscan. 1996. Facial soft-tissue thicknesses in the adult male Zulu. *Forensic Sci. Int*. 79:83–102.

Baillie, L. J., S. A. Mirijali, B. E. Niven et al. 2015. Ancestry and BMI influences on facial soft tissue depths for a cohort of Chinese and Caucasoid women in Dunedin, New Zealand. *J. Forensic Sci*. 60:1,146–1,154.

Baillie, L. J., J. C. Muirhead, P. Blyth et al. 2015. Position effect on facial soft tissue depths: A sonographic investigation. *J. Forensic Sci*. 61:S60–S70.

Beichel, R., E. Ulrich, C. Bauer et al. 2015. Data from QIN-HEADNECK. The Cancer Imaging Archive.

Bosch, W., W. Straube, J. Matthews et al. 2015. Data from Head-Neck_Cetuximab. The Cancer Imaging Archive.

Briers, N., T. Briers, P. Becker et al. 2015. Soft tissue thickness values for black and coloured South African children aged 6–13 years. *Forensic Sci. Int.* 252:188.e1–188.e10.

Bulut, O., C. Y. Jessica Liu, F. Koca et al. 2017. Comparison of three-dimensional facial morphology between upright and supine positions employing three-dimensional scanner from live subjects. *Leg. Med. (Tokyo)* 27:32–37.

Bulut, O., S. Sipahioglu, and B. Hekimoglu. 2014. Facial soft tissue thickness database for craniofacial reconstruction in the Turkish adult population. *Forensic Sci. Int*. 242:44–61.

Caple, J., and C. Stephan. 2016. A standardized nomenclature for craniofacial and facial anthropometry. *Int. J. Legal Med*. 130:863–879.

Caple, J., C. Stephan, L. Gregory et al. 2016. Effect of head position on facial soft tissue depth measurements obtained using computed tomography. *J. Forensic Sci*. 61:147–152.

Cignoni, P., M. Callieri, M. Corsini et al. 2008. MeshLab: An open-source mesh processing tool. Eurographics Italian Chapter Conference 2008:129–136.

Cignoni, P., C. Rocchini, and R. Scopigno. 1998. Metro: Measuring error on simplified surfaces. Computer Graphics Forum. 17:167–174.

Clark, K., B. Vendt, K. Smith et al. 2013. The Cancer Imaging Archive (TCIA): Maintaining and operating a public information repository. *J. Digit. Imaging* 26:1,045–1,057.

Codinha, S. 2009. Facial soft tissue thicknesses for the Portuguese adult population. *Forensic Sci. Int.* 184:80.e1–80.e7.

De Greef, S., P. Claes, D. Vandermeulen et al. 2006. Large-scale in-vivo Caucasian facial soft tissue thickness database for craniofacial reconstruction. *Forensic Sci. Int.* 159S:S126–S146.

de Almeida, N. H., E. Michel-Crosato, L. de Paiva et al. 2013. Facial soft tissue thickness in the Brazilian population: New reference data and anatomical landmarks. *Forensic Sci. Int.* 231:404.e1–404.e7.

Domaracki, M., and C. Stephan. 2006. Facial soft tissue thicknesses in Australian adult cadavers. *J. Forensic Sci*. 51:5–10.

Dong, Y., L. Huang, Z. Feng et al. 2012. Influence of sex and body mass index on facial soft tissue thickness measurements of the northern Chinese adult population. *Forensic Sci. Int*. 222:396.e1–396.e7.

Dumont, E. 1986. Mid-facial tissue depths of white children: An aid in facial feature reconstruction. *J. Forensic Sci*. 31:1,463–1,469.

El-Mehallawai, I. H., and E. M. Soliman. 2001. Ultrasonic assessment of facial soft tissue thicknesses in adult Egyptians. *Forensic Sci. Int*. 117:99–107.

Fedorov, A., R. Beichel, J. Kalpathy-Cramer et al. 2012. 3D Slicer as an image computing platform for the Quantitative Imaging Network. *Magn. Reson. Imaging* 30:1,323–1,341.

Fedorov, A., D. Clunie, E. Ulrich et al. 2016. DICOM for quantitative imaging biomarker development: A standards based approach to sharing clinical data and structured PET/CT analysis results in head and neck cancer research. *PeerJ*. 4:e2057.

Guyomarc'h, P., F. Santos, B. Dutailly et al. 2013. Facial soft tissue depths in French adults: variability, specificity and estimation. *Forensic Sci. Int*. 231:411.e1–411.e10.

Hazelden, A. 2014. MultiMeshScripting v1.0.1. Retrieved from Github: https://github.com/AndrewHazelden/MultiMesh-Scripting/releases/tag/v1.0.1.

His, W. 1895. Anatomische Forschungen über Johann Sebastian Bach's Gebeine und Antlitz nebst Bemerkungen über dessen Bilder. Bandes der Abhandlungen der Mathematisch-physischen Classe der Konigl. Sachsischen Gesellschraft der Wissenschaften. 22:380–420. In Stewart 1954 and Krogman and Iscan 1986.

Hodson, G., L. Lieberman, and P. Wright. 1985. In vivo measurements of facial tissue thicknesses in American Caucasoid children. *J. Forensic Sci*. 30:1,100–1,112.

Huculak, M., and T. Peckmann. 2012. In vivo facial tissue depth study of African Nova Scotian children. *Can. Soc. Forensic Sci. J.* 45:126–142.

Hwang, H., M. Park, W. Lee et al. 2012. Facial soft tissue thickness database for craniofacial reconstruction in Korean adults. *J. Forensic Sci*. 57:1,442–1,447.

Hwang, H., S. Choe, J. Hwang et al. 2015. Reproducibility of facial soft tissue thickness measurements using cone-beam CT images according to the measurement methods. *J. Forensic Sci.* 60:957–965.

Jeelani, W., M. Fida, and A. Shaikh. 2015. Facial soft tissue thickness among three skeletal classes in adult Pakistani subjects. *J. Forensic Sci.* 60:1,420–1,425.

Jia, L., B. Qi, J. Yang et al. 2016. Ultrasonic measurement of facial tissue depth in a Northern Chinese Han population. *Forensic Sci. Int.* 259:247.e1–247.e6.

Kirk, S., Y. Lee, C. Roche et al. 2016. Radiology data from The Cancer Genome Atlas Thyroid Cancer [TCGA-THCA] collection. The Cancer Imaging Archive.

Kotrashetti, V., and M. Mallapur. 2016. Radiographic assessment of facial soft tissue thickness in South Indian population--An anthropologic study. *J. Forensic Leg. Med.* 39:161–168.

Krogman, W., and M. Iscan. 1986. *The Human Skeleton in Forensic Medicine (2nd ed.).* Springfield, IL: Charles C. Thomas.

Manhein, M., G. Listi, R. Barsley et al. 2000. In vivo facial tissue depth measurements for children and adults. *J. Forensic Sci.* 45:48–60.

Panenková, P., R. Beňuš, S. Masnicová et al. 2012. Facial soft tissue thicknesses of the mid-face for Slovak population. *Forensic Sci. Int.* 220:293.e1–293.e6.

Parks, C., A. Richard, and K. Monson. 2014. Preliminary assessment of facial soft tissue thickness utilizing three-dimensional computed tomography models of living individuals. *Forensic Sci. Int.* 237:146.e1–146.e10.

Phillips, V., and N. Smuts. 1996. Facial reconstruction: Utilization of computerized tomography to measure facial tissue thickness in a mixed racial population. *Forensic Sci. Int.* 83:51–59.

Rhine, J., and H. Campbell. 1980. Thickness of facial tissues in American blacks. *J. Forensic Sci*. 25:847–858.

Rhine, J., and C. Moore. 1984. Tables of facial tissue thickness of American Caucasoids in forensic anthropology. Maxwell Museum Technical Series 1.

Ruiz, N. 2013. Facial soft tissue thickness of Colombian adults. *Forensic Sci. Int*. 229:160.e1–160.e9.

See, M., C. Roberts, and C. Nduka. 2008. Age- and gravity-related changes in facial morphology: 3-dimensional analysis of facial morphology in mother-daughter pairs. *J. Oral. Maxillofac. Surg*. 66:1,410–1,416.

Shrimpton, S., K. Daniels, S. de Greef et al. 2014. A spatially-dense regression study of facial form and tissue depth: Towards an interactive tool for craniofacial reconstruction. *Forensic Sci. Int.* 234:103–110.

Shui, W., M. Zhou, Q. Deng et al. 2016. Densely calculated facial soft tissue thickness for craniofacial reconstruction in Chinese adults. *Forensic Sci. Int*. 266:573.e1–573.e12.

Simmons-Ehrhardt, T., C. S. Falsetti, A. Falsetti et al. 2017. User guide: Dense facial tissue depth mapping of 3D CT models using Meshlab. *Figshare*.

Simmons-Ehrhardt, T., C. S. Falsetti, A. Falsetti et al. 2017. Fileset: Procedure for transforming 3D computed tomography (CT) skull and face models to a common orientation. *Figshare*.

Simpson, E., and M. Henneberg. 2002. Variation in soft-tissue thicknesses on the human face and their relation to craniometric dimensions. *Am. J. Phys. Anthropol*. 118:121–133.

Sipahioglu, S., H. Ulubay, and H. Diren. 2012. Midline facial soft tissue thickness database of Turkish population: MRI study. *Forensic Sci. Int*. 219:282.e1–282.e8.

Smith, S., and P. Buschang. 2001. Midsagittal facial tissue thicknesses of children and adolescents from the Montreal growth study. *J. Forensic Sci*. 46:1,294–1,302.

Starbuck, J., A. Ghoneima, and K. Kula. 2015. Facial tissue depths in children with cleft lip and palate. *J. Forensic Sci*. 60:274–284.

Stephan, C. 2017. 2018 tallied facial soft tissue thicknesses for adults and sub-adults. *Forensic Sci. Int.* 280:113–123.

Stephan, C., and E. Simpson. 2008. Facial soft tissue depths in craniofacial identification (part I): An analytical review of the published adult data. *J. Forensic Sci*. 53:1,257–1,272.

Stephan, C., and E. Simpson. 2008. Facial soft tissue depths in craniofacial identification (part II): An analytical review of the published sub-adult data. *J. Forensic Sci*. 53:1,273–1,279.

Stephan, C., and R. Preisler. 2018. In vivo facial soft tissue thicknesses of adult Australians. *Forensic Sci. Int.* 282:220.e1–220.e12.

Stewart, T. 1954. Evaluation of evidence from the skeleton. In *Legal Medicine,* R. Gradwohl, ed. St. Louis, MO: Mosby, 407–450.

Suzuki, K. 1948. On the thickness of the soft tissue parts of the Japanese face. *Anthropol. Sci.* 60:7–11.

TDMorpheus©. https://mirc.uzleuven.be/MedicalImageComputing/downloads/tdmorpheus.php.

Tu, P., R. Hartley, W. Lorensen et al. 2005. Face reconstructions using flesh deformation modes. In *Computer-Graphic Facial Reconstruction*, J. Clement and M. Marks, eds. Burlington, MA: Elsevier Academic Press, 145–162.

Turner, W., R. Brown, T. Kelliher et al. 2005. A novel method of automated skull registration for forensic facial approximation. *Forensic Sci. Int.* 154:149–158.

Utsuno, H., T. Kageyama, K. Uchida et al. 2014. Facial soft tissue thickness differences among three skeletal classes in Japanese population. *Forensic Sci. Int*. 236:175–180.

Vandermeulen, D., P. Claes, D. Loeckx et al. 2006. Computerized craniofacial reconstruction using CT-derived implicit surface representations. *Forensic Sci. Int*. 159S:S164–S174.

Wilkinson, C. 2002. In vivo facial tissue depth measurements for white British children. *J. Forensic Sci.* 47:459–465.

Williamson, M., S. Nawrocki, and T. Rathbun. 2002. Variation in midfacial tissue thickness of African-American children. *J. Forensic Sci.* 47:25–31.

Zuley, M., R. Jarosz, S. Kirk et al. 2016. Radiology data from The Cancer Genome Atlas Head-Neck Squamous Cell Carcinoma [TCGA-HNSC] collection. The Cancer Imaging Archive.

Table 1. CT Sample Utilized for Dense FTDMs, Including Duplicate Individuals

	Individuals	Scans	Minimum Age	Maximum Age
Females	43	46	21	80
Males	63	66	39	82
Total	106	112		

Figure 1.

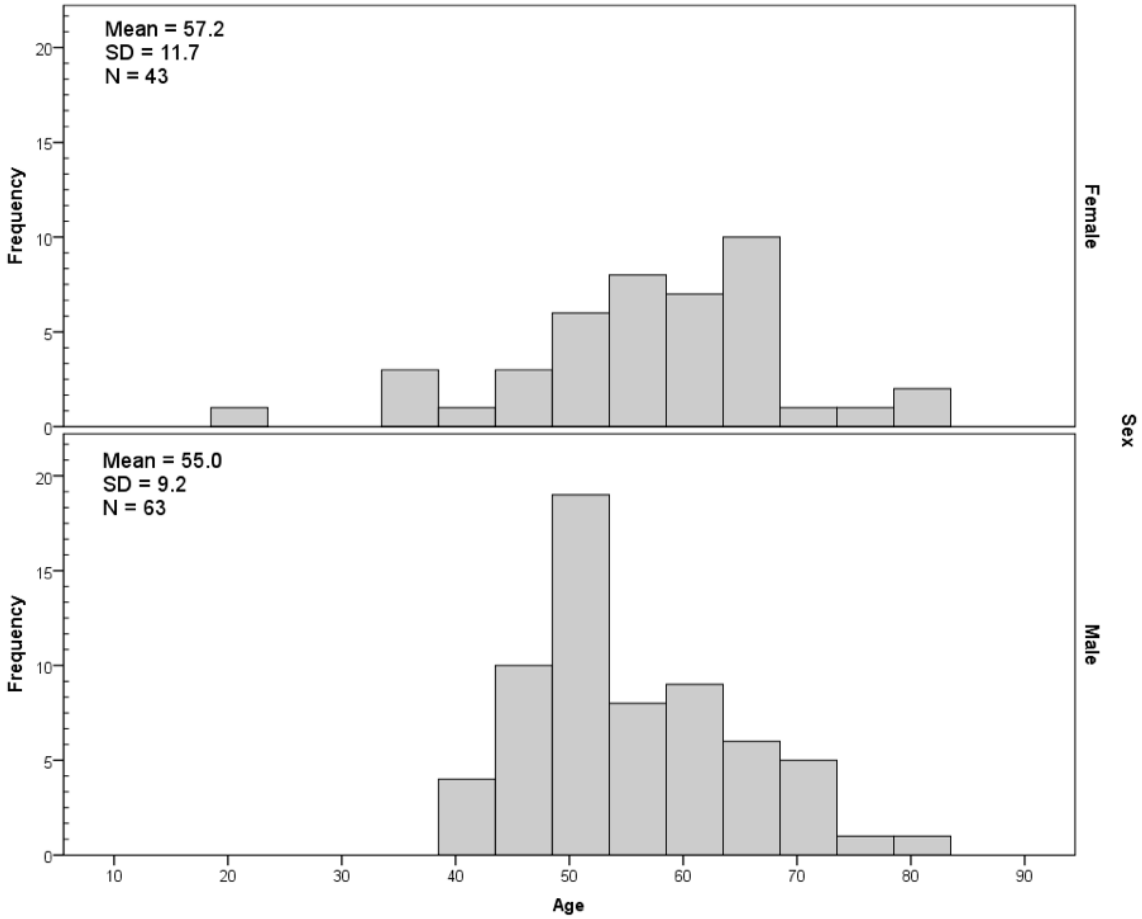

Figure 2.

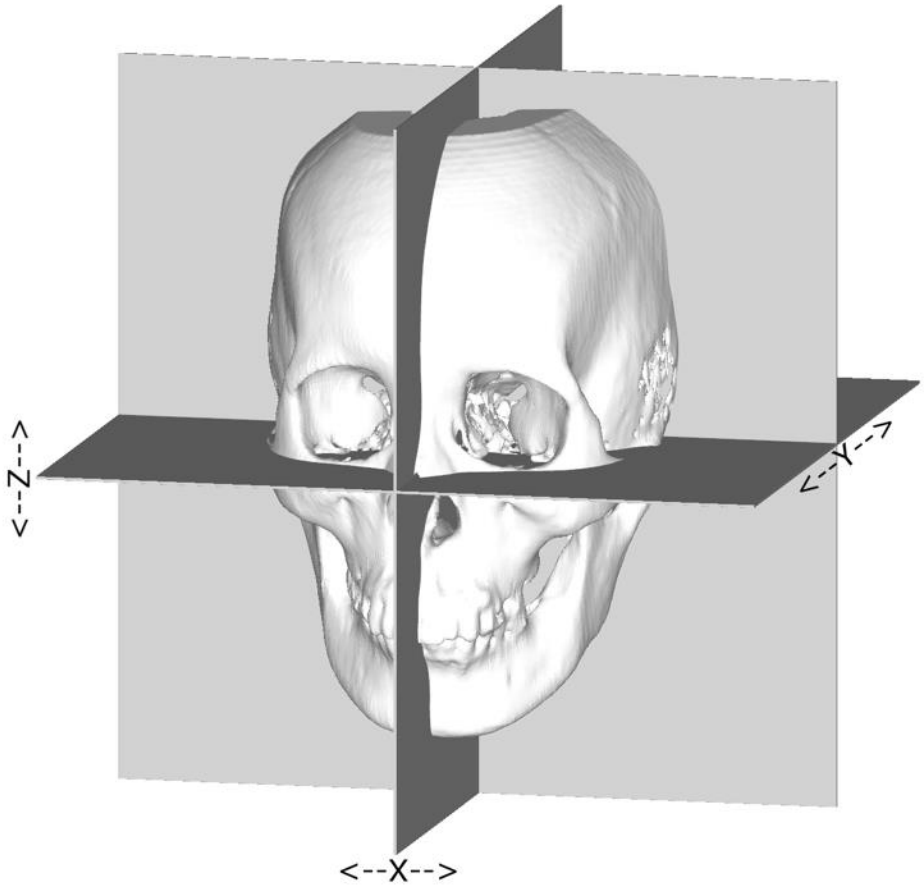

Figure 3.

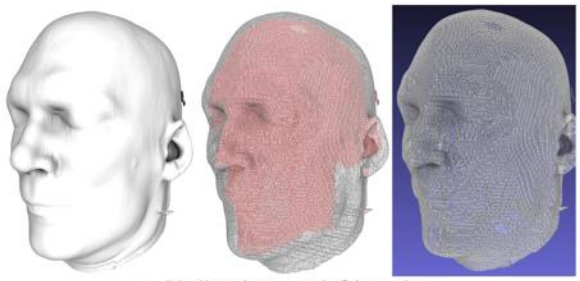

a. Hollowing and Cleaning

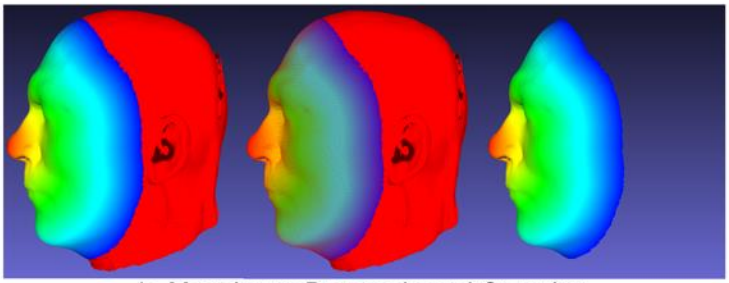

b. Mapping to Pronasale and Cropping

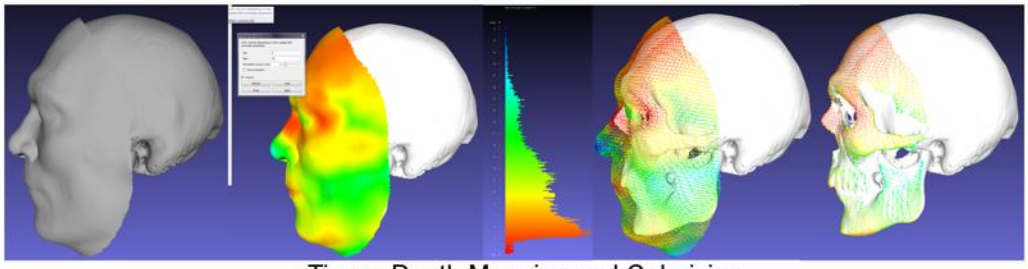

c.Tissue Depth Mapping and Colorizing

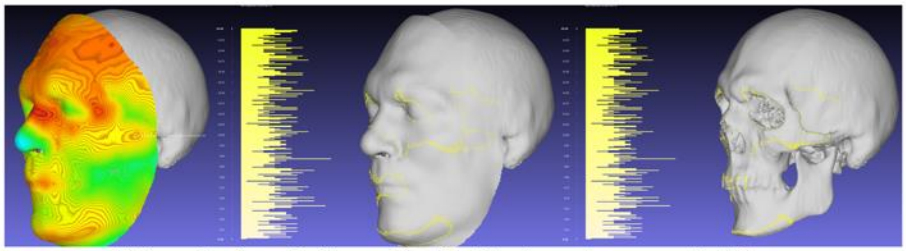

d.Visualization Options: Quality Contour, Incremental Maps

Figure 4.

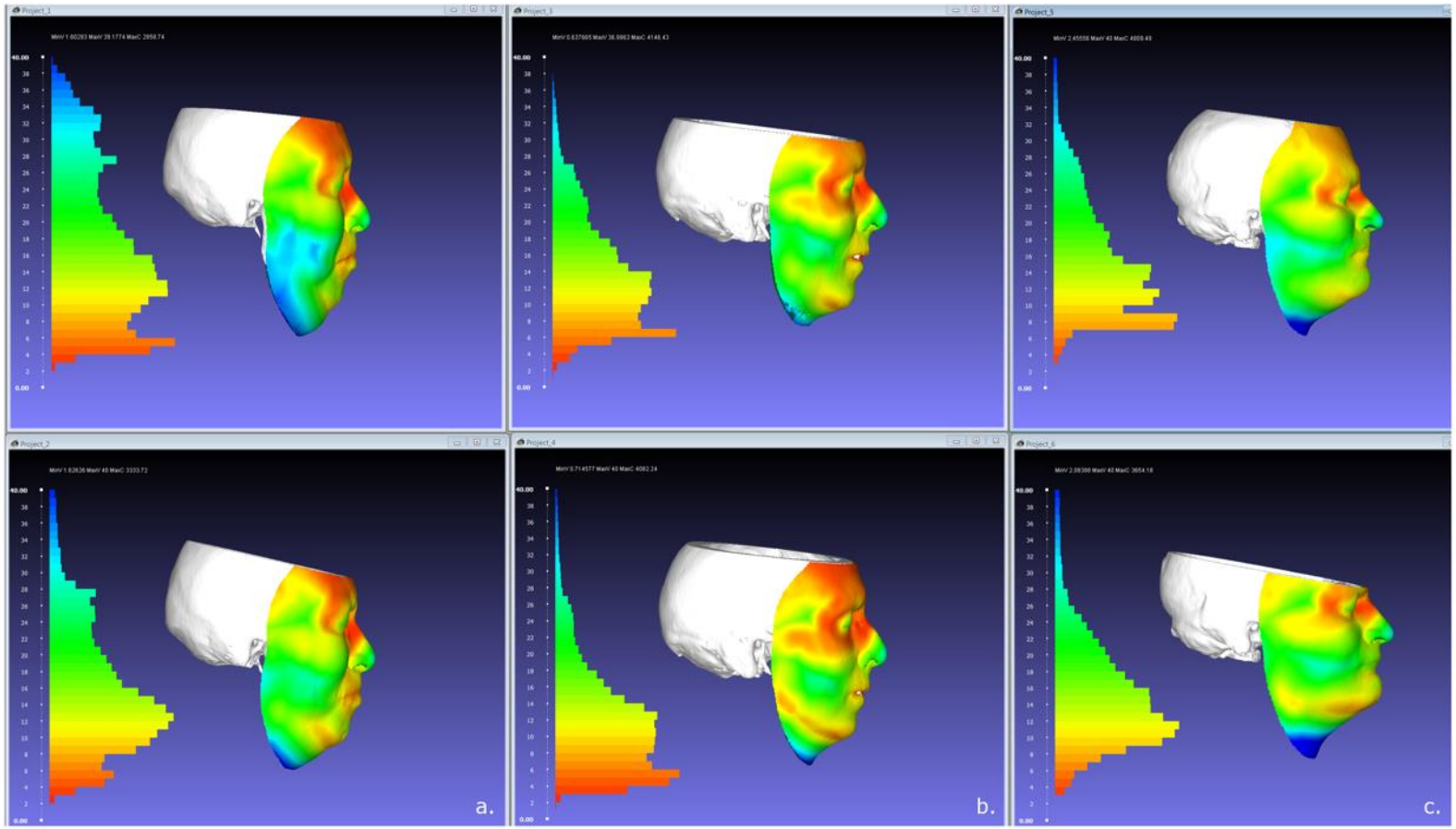

Figure 5.

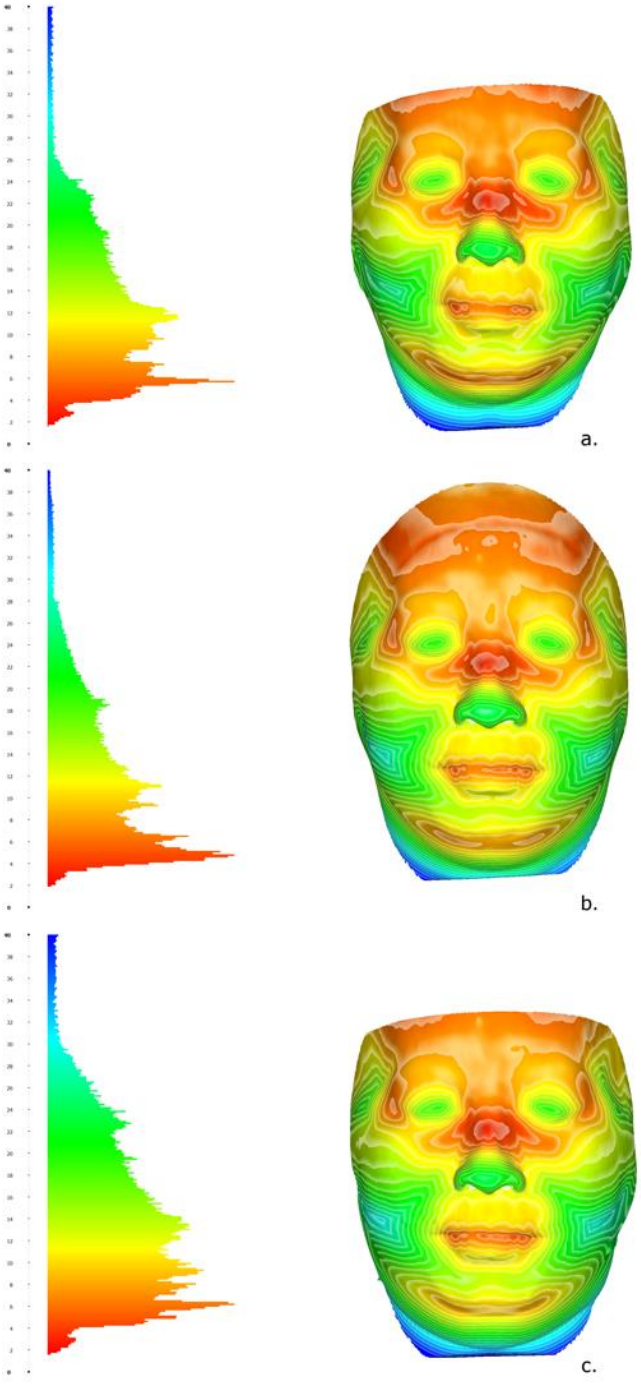

Figure 6.

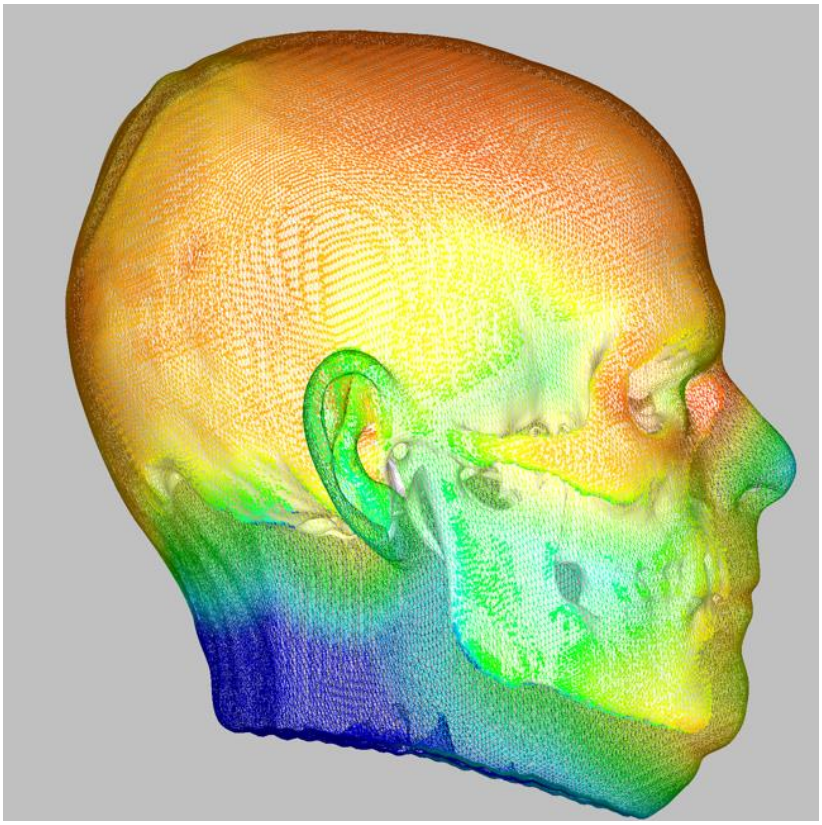

Figure 7.

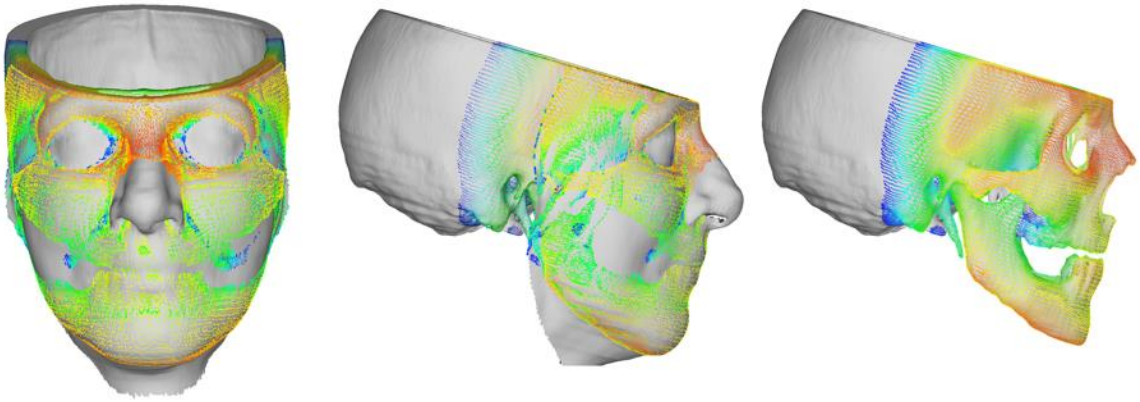

Figure 8.

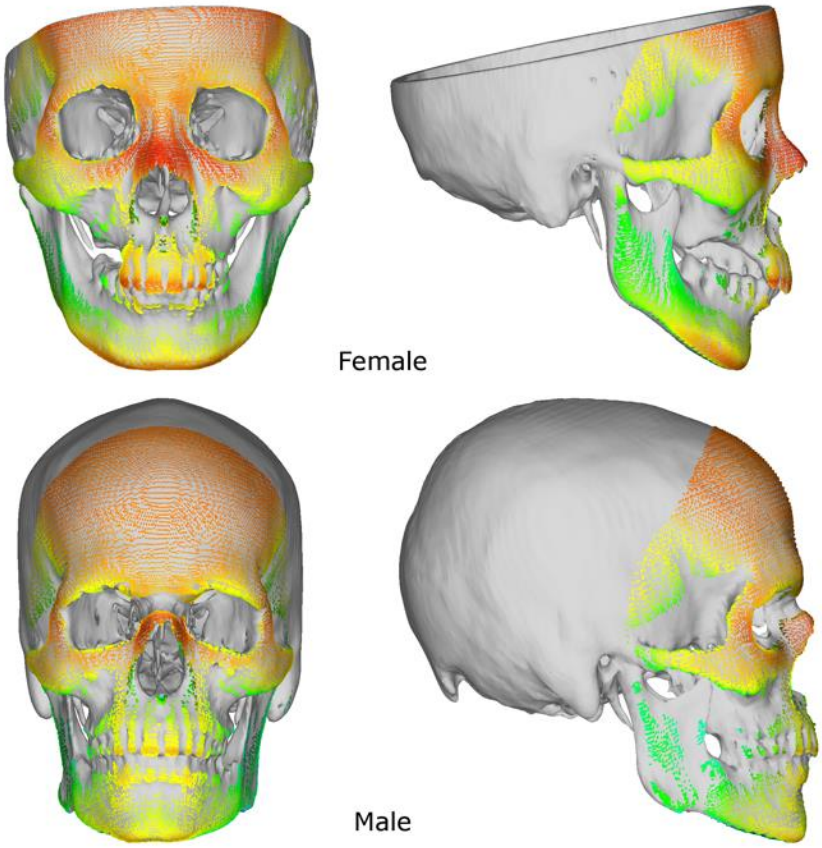

Figure Captions

Figure 1. Age distribution of the sample.

Figure 2. Orientation and coordinate system. The x-axis defines the medial-lateral direction with the mid-sagittal plane at N at x = 0. The y-axis defines the anterior-posterior direction with PoL and PoR defining a coronal plane at y = 0. The z-axis defines the superior-inferior direction with the Frankfurt Horizontal plane (OrL, PoL, PoR) at z = 0.

Figure 3. Summary of steps for dense facial tissue depth mapping (FTDM). a) hollowing and cleaning, b) mapping to pronasale and cropping face, c) tissue depth mapping and colorization, d) visualization options: quality contour, incremental maps (example shows the 10.0 mm face points and skull points in yellow).

Figure 4. Three individuals with scans at visibly different weights. Top row contains the "heavier" face. Histograms show the distribution of facial depths from 0.0 to 40.0 mm depth, colorized from red (thinnest) to blue (thickest).

Figure 5. One individual with three different weights. The "Quality Contour" feature in Meshlab was applied to the FTDMs to enhance visualization of depth transitions.

Figure 6. Example FTDM of a full hollowed face shell, rather than a cropped face shell.

Figure 7. Result of mapping from skull to face utilizing the Hausdorff sampling filter. Note that the gray portions of the face were unmapped.

Figure 8. Comparison of skull points generated for female and male skulls to depict the differences in curvature that would affect geometric measurements as well as tissue depth marker placement.